ChemPubSoc Europe

DOI: 10.1002/batt.201800072

BATTERIES & SUPERCAPS Communications

VIP *Very Important Paper*

Doping Graphene into Monodispersed Fe_3O_4 Microspheres with Droplet Microfluidics for Enhanced Electrochemical Performance in Lithium-Ion Batteries

Na Liu,[a] Chunlin Li,[a] Hua Xie,[a] Yingjia Liu,[a] Jiannan Liu,[a] Jing Gao,[a] Jingfeng Han,[a] Jian Chen,[a] Yingxu Wei,[a] Bingcheng Lin,[a] and Zhongmin Liu*[a]

Graphene-doped Fe_3O_4 monodispersed microspheres are fabricated utilizing a droplet microfluidic technology. The electrochemical performance of the Fe_3O_4 microspheres as anode material for Li-ion batteries is enhanced by doping trace graphene in the droplet reactor. The discharge capacity remains 550 mAh/g at 0.1 C after 190 cycles, which is 2 times higher than that of the graphene doped Fe_3O_4 samples prepared by the traditional precipitation method, and 5 times higher than that of pure Fe_3O_4 after 100 cycles. The uniform droplet reactor in form of a droplet microfluidic chip might provide a homogeneous microscopic condition for in-situ electrostatic co-assembly of the positive-charged Fe colloids and the negative-charged graphene oxide sheets to shape a homogeneous solid framework, resulting in homogeneously doping trace graphene into the Fe_3O_4 microspheres.

Fe_3O_4 as an anode material of Li-ion batteries (LIBs) has attracted much attention due to its high theoretical storage capacity (926 mAh/g), low cost, environment friendly and natural abundance.[1] Unfortunately, its practical utilization suffers severe capacity degradation arising from the large volume change (ca. 200% volume increase) and the aggregation of Fe_3O_4 nanoparticles during the charge/discharge circling processes.[2] Nanostructured materials have better accommodation for the strains of Li insertion/extraction,[3] so many researches have designed nanomaterials with diverse morphologies such as nanospheres,[4] nanospindles,[5] core-shell nanosheets,[2b] or hollow sphere,[6] which showed the improving capacity of metal oxides materials for LiBs.[3,7] However, it was found that nanostructured materials might be broken or aggregated after several discharge/charge cycles, which led to severely capacity fading.[2b,c,5,8] One generally accepted strategy to alleviate these problems is to load nanomaterials into a carbon-based matrix to protect their nanostructures from harm during discharge/charge processes.[5,8a,9] Among many carbon matrices, graphene (GN) has drawn great attention due to its excellent electrical conductivity, high thermal and chemical stability, large surface area, and unique planar structure.[10] Considerable researches modified Fe_3O_4 nanoparticles with graphene by using different strategies, including depositing Fe_3O_4 nanoparticles on graphene sheets,[8a,d,e,11] embedding Fe_3O_4 nanoparticles/microspheres into the conductive graphene matrix,[2c,12] graphene encapsulating Fe_3O_4 nanospheres,[4b,9a,13] crosslinking Fe_3O_4 nanoparticles into graphene sponge[14] and so on. In all these efforts, a huge amount of graphene sheets (from 5% in Jiao' work[15] to 77% in Li's work[16]) seems to be necessary for improving the electrochemical performances. It seems reasonable that plenty of graphene was benefit to well isolate Fe_3O_4 nanoparticles from self-aggregation and large volume change, resulting in better cycling stabilities.[2c,4b,8a,13a] However, due to the strong Vander Waals force, graphene itself is apt to aggregate into a bulky form, which leads to a severely reduced effective specific surface area and the increased resistance for Li^+ to reach the core of active materials, and thereby causes the strictly reduced electrochemical capacity of Fe_3O_4.[8a,10] It was approved by Sathish et al[8c] that high graphene content did not bring about the optimal capacity performance and cycle stability when they investigated the electroactivity of Fe_3O_4/graphene composites with different weight ratios. Liu[2c] also got a similar result. Besides, considering that graphene is more expensive but has lower theoretical capacities than Fe_3O_4, it is reasonable that instead of using high content graphene, improving the utilization efficiency of graphene in the Fe_3O_4/graphene composite could be expectable to enhance the electroactivity of Fe_3O_4 electrodes for LIBs.

Droplet microfluidics is one of the most promising approaches to produce and functionalize monodisperse particles through the preparation of uniform droplets with a wide range of size from nanometers to millimeters.[17] Typically, each droplet can be performed as a highly identical micro/nanoscale reactor in the microchannel. Due to the short dynamics diffusion distance in a tiny droplet, it could readily achieve a high mixing performance and an identical microcosmic environment.[17b,18] Considering these advantages of the droplet microfluidics, we propose that doping trace graphene into Fe_3O_4 materials with droplet microfluidics might achieve the highly efficient utilization of graphene in the Fe_3O_4/graphene composite, and thereby enhance the electrochemical performance of Fe_3O_4. Herein, such graphene doped Fe_3O_4 monodispersed microspheres were synthesized and their electrochemical performances were evaluated.

[a] *Dr. N. Liu, Dr. C. Li, Dr. H. Xie, Dr. Y. Liu, Dr. J. Liu, Dr. J. Gao, Dr. J. Han, Dr. J. Chen, Dr. Y. Wei, Prof. B. Lin, Prof. Z. Liu*
Dalian Institute of Chemical Physics,
Chinese Academy of Sciences,
457 Zhongshan Road, Dalian, 116023, China
E-mail: zml@dicp.ac.cn

Supporting information for this article is available on the WWW under https://doi.org/10.1002/batt.201800072

As shown in Figure 1, the synthetic procedure with droplet microfluidic consists of four steps, droplet formation, pre-solidification, evaporation and calcination. Firstly, the monodispersed droplets of Fe ions and graphene oxide mixture were formed by hydrodynamics flow focusing in the droplet-generating unit of the microfluidic device (Figure S1). The dispersion phase was an aqueous mix solution containing of $Fe(NO_3)_3$ and trace graphene oxide (GO). The continuous phase was a mineral oil containing 4 wt% EM90 as surfactant. The monodisperse microspheres were prepared by precisely adjusting the introducing rate and amount of the precipitating agent using the microfluidic device (Figure S2). Secondly, the monodisperse droplets were subsequently solidified by introducing precipitant to the droplets in the downstream solidification unit of microfluidic device (Figure S1). 7.5 wt% Triethanolamine (TEA) was added into the continuous phase to obtain a precipitation phase and TEA was also a reducing agent. After solidification unit, the pre-solidified droplets had an average diameter of 221 μm and a coefficient of variation (CV) of 2.6% (Figure S3 (a)). The pre-solidified droplets were collected on a glass plate and transferred to an oven at 100 °C, wherein the water in the droplet was evaporated and a concentrated uniform microsphere was obtained. The microspheres diameters were shrinked to about 60 μm and the coefficient of variation was 4.1%, continuing to have the terrible homogeneity (Figure S3 (b)). After washed with hexane, ethanol and deionized water, the microspheres were treated at 800 °C under nitrogen atmosphere for 2 h, and finally the graphene-doped Fe_3O_4 microspheres (named as M–Fe_3O_4/GN) were obtained. During washing, some microspheres were adhered together, resulting in a larger coefficient of variation (18%) of final production (Figure S3 (c)).

In the uniform microscale droplets, a homogeneous reaction condition could be readily achieved. The graphene oxide sheets were negatively charged and constituted a micro matrix in the initial droplets. When droplets passed through the solidification unit, a proper amount of alkaline reagent (TEA) in the precipitation phase diffused into the droplets from the interface of droplet/oil to form Fe colloid nanoparticles. At this moment, the assembly of the positively-charged Fe colloid nanoparticles and the negatively-charged GO sheets by electrostatic interaction dominated the precipitation procedure instead of the precipitation reaction of Fe colloids, and a solid framework was constructed in the droplet with a dimension of thousands of picoliter. In this uniform picoliter-scale volume, the Fe gelling reaction and following electrostatic assembly with graphene oxide sheets readily developed homogeneously. Due to the identical conditions including temperature and concentration, the formation of inhomogeneous nanoparticles and the self-aggregation of graphene sheets could be avoided, and consequently the graphene homogeneously doping into Fe components was achieved. For comparison, a graphene doped Fe_3O_4 sample (named as T–Fe_3O_4/GN) with the same compositions as M–Fe_3O_4/GN sample was prepared with a conventional precipitation method in a bulk reactor. Besides, a pure Fe_3O_4 sample (name as M–Fe_3O_4) was also prepared by droplet microfluidics. As shown in the images of Figure S4, distinctly difference from the monodisperse form of M–Fe_3O_4/GN microspheres, T–Fe_3O_4/GN sample shows an imhomogeneous form while M–Fe_3O_4 sample appears to be aggregated.

The characterization results of the M–Fe_3O_4/GN, T–Fe_3O_4/GN and M–Fe_3O_4 samples are shown in Figure 2. From Figure 2 (a), the X-ray diffraction (XRD) peaks in all three samples are assigned to Fe_3O_4 phase (Fe_3O_4-JCPDS No. 19-0629). Other peaks (at 26 °C and 45 °C) in the T–Fe_3O_4/GN sample is assigned to the diffraction peaks of γ-Fe_2O_3 ($Fe_{21.333}O_{32}$, 98-001-8032), which was formed by calcination at high temperatures of trivalent Fe oxides.[19] No peak assigned to graphene was observed in both containing GN samples due to the ultra-low loading of graphene. The Raman spectroscopy was further investigated for confirming the presence of graphene. The characteristic D and G bands of graphene sheets are observed at ~1340 and 1590 cm^{-1} (Figure 2 (b)), which are in correspondence with the reported values in the literatures,[2c,11,20] indicating that the graphene presences in both samples. The amounts of graphene in M–Fe_3O_4/GN and T–Fe_3O_4/GN samples were estimated by thermogravimetric analysis (TG) (Figure 2 (c)). The graphene contents estimated from the combustion of graphene from 300 °C to 550 °C in both samples are about 0.2 wt%.[21]

The morphology of M–Fe_3O_4/GN microsphere was investigated by SEM (Figure 3a, b, c) and TEM (Figure 3j). The solid microsphere consisted of Fe_3O_4 nanoparticles with uniform size of a dozen of nanometers. As shown in SEM images of

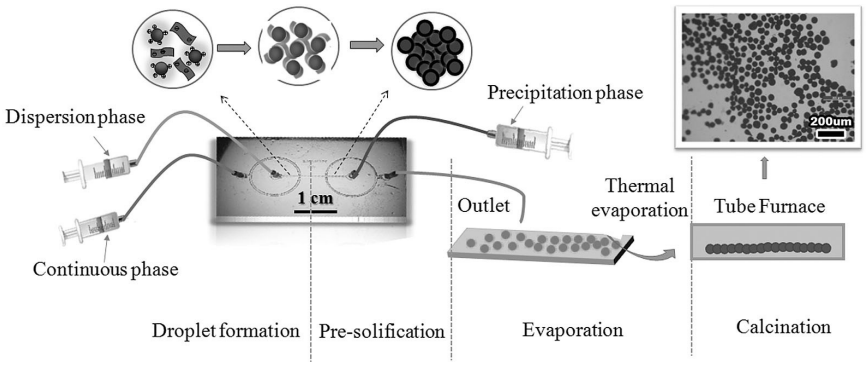

Figure 1. The fabrication process of M–Fe_3O_4/GN microspheres.

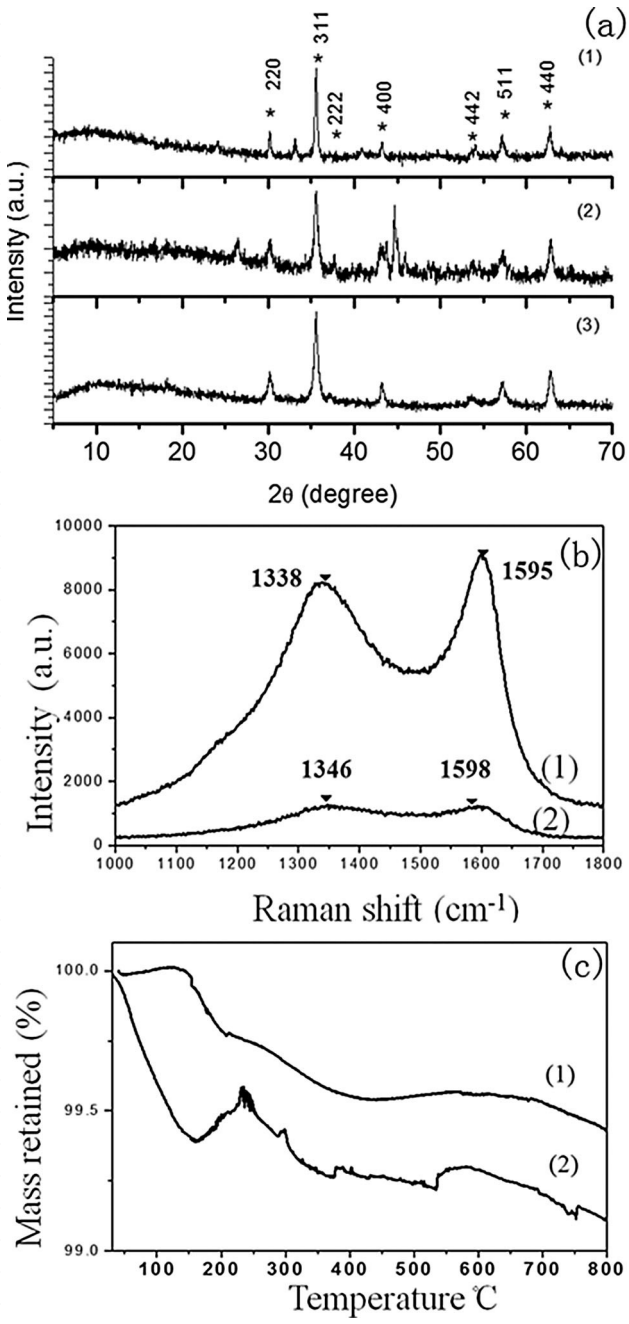

Figure 2. a) XRD profiles, b) Raman spectra and c) TG profiles of the samples. (1) M–Fe_3O_4/GN; (2) T–Fe_3O_4/GN and (3) M–Fe_3O_4.

M–Fe_3O_4/GN (Figure 3a, b, c), these Fe_3O_4 nanoparticles were assembled into an incompact aggregation and some with misty boundaries, revealing that the graphene was probably embedded among nanoparticles. The typical TEM image (Figure 3j) reveals that uniform-size Fe_3O_4 nanoparticles with a size of around 20 nm decorated efficiently with thin graphene sheets were loosely assembled together in M–Fe_3O_4/GN sample, and free graphene sheet was rare to be observed, which is consistent with the SEM results. While for the SEM (Figure 3d, e, f) and TEM (Figure 3k) of T–Fe_3O_4/GN sample, uneven-size Fe_3O_4 particles with sizes from 10 nm to 300 nm were observed. Although partial Fe_3O_4 particles were enwrapped by thick graphene sheets, undecorated Fe_3O_4 particles and free graphene sheets were also presented. It suggests that difference from the droplet microfluidic method, the precipitation reaction of Fe dominated the preparation procedure instead of assembling interaction between Fe and graphene when adding TEA into the bulky solution, which led to the formations of inhomogeneous Fe_3O_4 nanoparticles and weak assembling of Fe and graphene. From the SEM (Figure 3g, h, i) and TEM image (Figure 3 l) of the M–Fe_3O_4 sample, the microsphere was compactly stacked with homogeneous Fe_3O_4 nanoparticles with a size of a dozen of nanometer.

From above characterization results, it is concluded that compared with the conventional bulky precipitation method, droplet microfluidics is prone to obtain the homogeneous Fe_3O_4/GN composites, including uniform-size Fe_3O_4 nanoparticles and the homogenously doping of graphene sheets. This is probably because the monodisperse droplet produced by microfluidic chip could act as a picoliter-scale reactor, wherein a short thermodynamic diffusion distance could ensure a homogeneous microscopic reaction condition, and consequently the Fe gelling reaction and its electrostatic co-assembly with GO sheets undergo in a stable way. As for the bulky precipitation method, the large reaction volume brings out enormous local differences of reaction conditions, such as temperature, concentration and pH, resulting in the formation of nonuniformed Fe_3O_4 nanoparticles and inhomogeneous co-assembly with GO sheets. For lithium-ion batteries, the homogeneity of electrode material is crucial to achieve a better electrochemical performance.

The cyclic voltammograms (CVs) of M–Fe_3O_4/GN sample for the first five cycles at a scan rate of 0.1 mV/s with the cutoff voltages between 0.01 and 3.0 V were obtained and plotted in Figure 4 (a). In the cathodic process, the reduction peak at 0.75 V was attributed to the reversible conversion of Fe_3O_4 to Fe and the formation of amorphous Li_2O.[22] After the first negative scan, this peak shifts to a higher voltage 0.8 V, indicating that there was an irreversible structural phase transformation during the lithium ion insertion and extraction in the initial cycle. The positive scan shows three peaks (at 1.6 V, 1.9 V and 2.3 V), which are corresponded to the oxidation reactions of Fe(0)/Fe(II), Fe(II)/Fe(III), and Fe(0)/Fe(III)respectively.[13a,22,23] The cathodic peak at 1.7 V might be ascribed to the lithium insertion into the structure of anodic materials.[24] The broaden cathodic peak at 2.1 V, which occurred in the first cycle but disappeared in the subsequent cycles, could be attributable to the formation of the SEI film and the decomposition of electrolyte in the circle process, which has been widely reported for transition metal oxides.[14,25] The galvanostatic discharge-charge performance of M–Fe_3O_4/GN electrode was measured at a current density of 0.1 C (94.2 mA/g) up to 5 cycles and shown in Figure 4 (b), together with that of T–Fe_3O_4/GN sample. M–Fe_3O_4/GN sample shows higher initial discharge (1302 mAh/g) and charge capacities (938 mAh/g) with an initial Coulombic efficiency of 72%, which are significantly higher than those of T–Fe_3O_4/GN sample (971 mAh/g, 494 mAh/g and 51%, respectively). Additionally, the Coulombic efficiency of

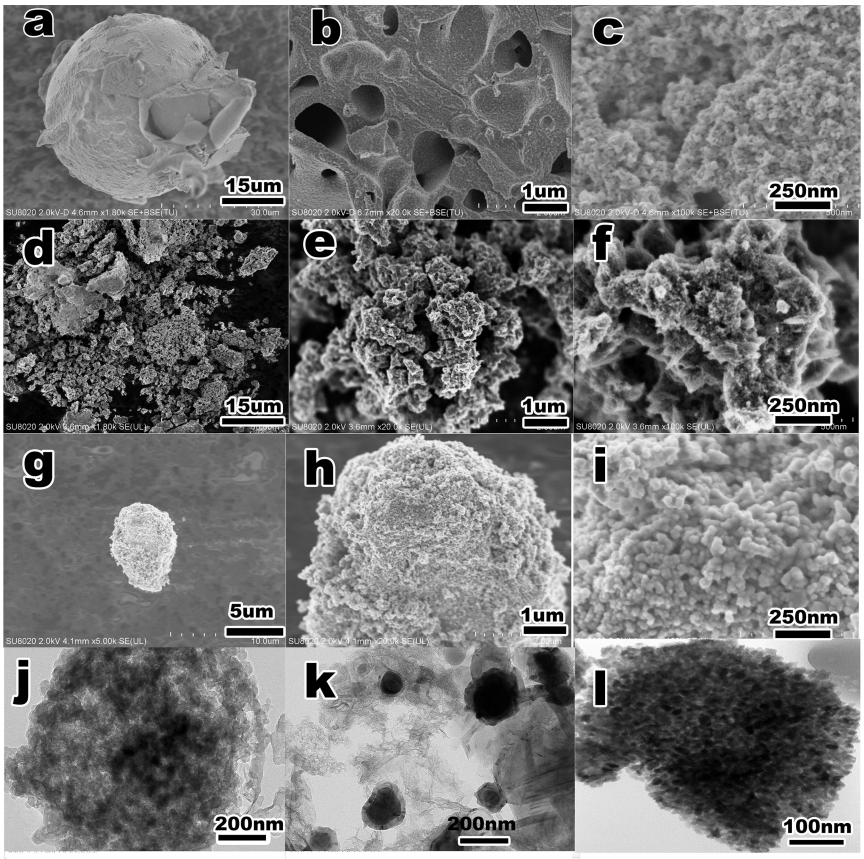

Figure 3. a), b), c) SEM images of M–Fe_3O_4/GN microsphere; d), e), f) SEM images of T–Fe_3O_4/GN sample; g), h), i) SEM images of M–Fe_3O_4 sample and TEM images of M–Fe_3O_4/GN (j), T–Fe_3O_4/GN (k) and M–Fe_3O_4 (l) samples.

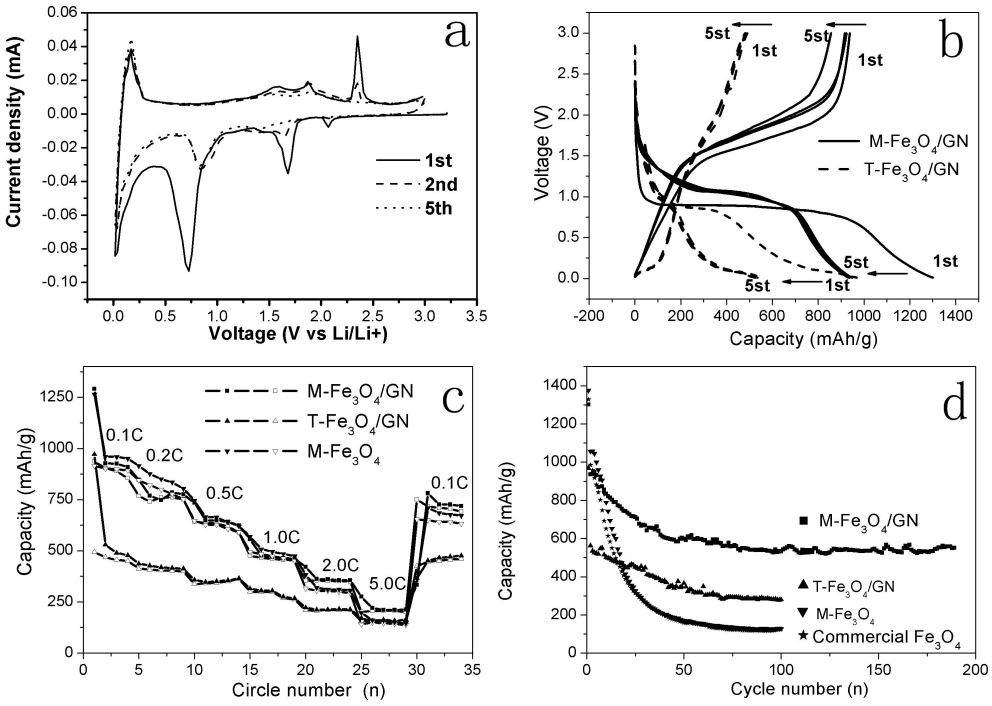

Figure 4. a) Cyclic voltammetry (CV) curves of M–Fe_3O_4/GN sample; b) Voltage profiles of M–Fe_3O_4/GN and T–Fe_3O_4/GN samples cycled at the current of 0.1 C; c) Rate performances of M–Fe_3O_4/GN, T–Fe_3O_4/GN and M–Fe_3O_4 samples (solid symbols for discharge capacities, hollow symbols for charge capacities); d) Cycling performances of M–Fe_3O_4/GN, T–Fe_3O_4/GN, M–Fe_3O_4 and commercial purchased Fe_3O_4 samples at the current of 0.1 C.

M–Fe_3O_4/GN sample rapidly increased to 99% in the second cycle, and remained around this value in the following cycles, which is distinctly higher than 88% for T–Fe_3O_4/GN sample. Higher Coulombic efficiencies of M–Fe_3O_4/GN than T–Fe_3O_4/GN suggests that the former has higher reversible Li storage capacity.

The rate performances of M–Fe_3O_4/GN, T–Fe_3O_4/GN and M–Fe_3O_4 electrodes were cycled from 0.1 C to 5.0 C and back to 0.1 C and the obtained results are shown in Figure 4 (c). It clearly shows that both samples prepared by droplet microfluidics (M–Fe_3O_4/GN and M–Fe_3O_4) exhibited superior rate capacities at various current densities from 0.1 C to 5.0 C compared with T–Fe_3O_4/GN sample prepared by the conventional method, illustrating the advantage of the microfluidics method. The cycle performances of two graphene-doped Fe_3O_4 samples (M–Fe_3O_4/GN and T–Fe_3O_4/GN samples), as well as two graphene-free Fe_3O_4 samples synthesized by microfluidic chip and commercial purchased were tested at a current rate of 0.1 C (showed in Figure 4 (d)). For pure Fe_3O_4, it is noticeable that M–Fe_3O_4 sample has a higher specific capacity than the commercial purchased Fe_3O_4 sample in the first 30 circles. After that, the capacities of both samples have almost the same fading tendency, decreasing quickly and retaining only ~120 mAh/g after 100 cycles. It illustrates that microfluidic method could improve the electroactivity properties of Fe_3O_4, although it is incapable of promoting the cycle performances of pure Fe_3O_4. Probably the microfluidic method affects the Fe_3O_4 nanoparticle size rather than its structure, and therefore the circle performance of obtained pure Fe_3O_4 (M–Fe_3O_4) was hardly promoted. For T–Fe_3O_4/GN sample, its cycle discharge capacity gradually decreased to 447 mAh/g in the first 30 cycles, and remained 281 mAh/g after 100 cycles, which is obviously higher than above pure Fe_3O_4 samples. It apparently attributes to that the doping graphene is benefit to improve the cycle performance of Fe_3O_4. For M–Fe_3O_4/GN sample, its discharge capacity gradually decreased to 654 mAh/g in the first 30 cycles, but remained at 550 mAh/g after 190 discharge-charge cycles, which is 5 times higher than that of pure Fe_3O_4 samples, and 2 times higher than that of T–Fe_3O_4/GN sample after 100 cycles. It clearly reveals that both capacity and cycle performance of graphene-doped Fe_3O_4 sample were promoted significantly by droplet microfluidic technology.

As demonstrated by the TEM images in Figure 3j, k, i, the Fe_3O_4 nanoparticles of M–Fe_3O_4 sample without doping graphene are compactly stacked and aggregated. While by doping graphene, the layer folding property of graphene nanosheets is helpful to prevent Fe_3O_4 nanoparticles from compact aggregation, which apparently improves the circle performance of Fe_3O_4. During charge/discharge processes, the doped graphene nanosheet not only acts as a conductor for electron transfer but also serves as a steady separator to prevent Fe_3O_4 particles from aggregating.[4b,8a,9a] Besides, comparing to the conventional bulky precipitation method, the more homogeneously doping effect of graphene sheets into monodispersed Fe_3O_4 microsphere by droplet microfluidic method, suggests the enhanced efficiency of graphene utilization, thereby leading to the outstandingly improving circle performance of graphene doped Fe_3O_4. Furthermore, the homogeneity of Fe_3O_4 nanoparticles was also improved by droplet microfluidic method, which brought a higher specific capacity. In brief, droplet microfluidic method improved the homogeneity of graphene-doped Fe_3O_4 composition materials, including the size homogeneity of Fe_3O_4 nanoparticles and the doping homogeneity of graphene, which is unattainable with conventional method, and eventually promoted the electrochemical performances of Fe_3O_4.

To further illustrate the specificity of current research, the performance comparison of Fe_3O_4/graphene materials with various graphene loading for LIBs is shown in Table 1. Although the loading amount of graphene (about 0.2 wt%) in current research is much lower than other researches, the retaining capacity of graphene doped Fe_3O_4 microspheres prepared with microfluidic chip showed a competitive or even better performance, demonstrating the superiority of current method.

In summary, graphene doped Fe_3O_4 monodisperse microspheres were fabricated in a droplet reactor with microfluidic technology. Comparing to the traditional bulky reactor, this uniform picoliter-scale droplet reactor provides a homogeneous thermodynamics environment for Fe Gelling reaction and electrostatic co-assembly of positively-charged Fe colloids and negatively-charged GO sheets to form graphene homogeneously doped Fe_3O_4 monodisperse microspheres. The rate performance and cycle capability of this graphene doped Fe_3O_4 as anode material were distinctly enhanced. They also showed competitive or even better cycle performance compared with some other Fe_3O_4/graphene materials containing of high content graphene, suggesting the improved utilization efficiency of graphene by microfluidic method. Such method of doping graphene into nanomaterials can be further extended to other metal oxides for energy storage and conversion applications.

Table 1. Comparison of various Fe_3O_4/graphene materials for LIBs.

Materials	Graphene percentage composition [wt.%]	Current density [mA/g]	Cycle number	Retaining capacity [mA/g]	References
Fe_3O_4/graphene	66.7	100	50	324	[2c]
Graphene-Wrapped Fe_3O_4	13.3	700	100	580	[26]
Fe_3O_4/N-doped graphene	5	100	50	593	[15]
Fe_3O_4/Graphene	60	50	50	675	[8c]
Graphene-Encapsulated Fe_3O_4	16.9	100	100	542	[13a]
Graphene-doped Fe_3O_4 microspheres	~0.2	94.2	190	550	This work

Experimental Section

Detailed synthetic methodologies and full characterizations of M–Fe_3O_4/GN, T–Fe_3O_4/GN and M–Fe_3O_4 samples are fully described in the Supporting information.

The working electrodes consisted of active materials, a conductive agent (acetylene black), and a polymer binder (poly(vinylidene difluoride), PVDF, Aldrich) in a 70:20:10 weight ratio. Then, the slurries of the mixture were cast onto an aluminum foil current collector and dried at 80 °C for 6 h to remove the solvent in an Ar-filled glovebox with concentrations of moisture and oxygen below 1.0 ppm. The electrodes were pressed at 1 MPa in the form of disks typically with a diameter of 10 mm. The electrolyte solution was 1 M LiPF6-ethylene carbonate (EC)/diethyl carbonate (DMC)/ethyl methyl carbonate (EMC) (1:1:1 by volume). The electrochemical tests of the samples were performed using an automatic battery testing system (LAND CT2001A model) at different current rates with a voltage window of 0.01 ~ 3.0 V and a constant temperature of 25 °C.

Acknowledgements

The authors gratefully acknowledge the supports of National Natural Science Foundation of China (No. 21376233). We wish to thank Prof. Jun Bao for TEM assistance.

Conflict of Interest

The authors declare no conflict of interest.

Keywords: droplet microfluidics · Fe_3O_4 · graphene · lithium-ion batteries · materials science

[1] J. S. Yeoh, C. F. Armer, A. Lowe, *Mater. Today Energy* **2018**, *9*, 198.
[2] a) Y. Wu, Y. Wei, J. P. Wang, K. L. Jiang, S. S. Fan, *Nano Lett.* **2013**, *13*, 818; b) Z. Zhang, F. Wang, Q. An, W. Li, P. Wu, *J. Mater. Chem. A* **2015**, *3*, 7036; c) Y. Liu, Y. Zhan, Y. Ying, X. Peng, *New J. Chem.* **2016**, *40*, 2649; d) Y. Liu, P. Li, Y. W. Wang, J. Y. Liu, Y. Wang, J. Q. Zhang, M. B. Wu, J. S. Qiu, *J. Alloys Compd.* **2017**, *695*, 2612; e) Q. H. Wu, R. F. Zhao, W. J. Liu, X. Zhang, X. Shen, W. L. Li, G. W. Diao, M. Chen, *J. Power Sources* **2017**, *344*, 74.
[3] Y. Lu, L. Yu, X. W. Lou, *Chem.* **2018**, *4*, 972.
[4] a) J. S. Chen, Y. Zhang, X. W. Lou, *ACS Appl. Mater. Interfaces* **2011**, *3*, 3276; b) W. Wei, S. Yang, H. Zhou, I. Lieberwirth, X. Feng, K. Mullen, *Adv. Mater.* **2013**, *25*, 2909.
[5] W. M. Zhang, X. L. Wu, J. S. Hu, Y. G. Guo, L. J. Wan, *Adv. Funct. Mater.* **2008**, *18*, 3941.
[6] F. X. Ma, H. Hu, H. B. Wu, C. Y. Xu, Z. Xu, L. Zhen, X. W. David Lou, *Adv. Mater.* **2015**, *27*, 4097.
[7] P. Poizot, S. Laruelle, S. Grugeon, L. Dupont, J. M. Tarascon, *Nature* **2000**, *407*, 496.
[8] a) P. C. Lian, X. F. Zhu, H. F. Xiang, Z. Li, W. S. Yang, H. H. Wang, *Electrochim. Acta* **2010**, *56*, 834; b) X. Li, X. Huang, D. Liu, X. Wang, S. Song, L. Zhou, H. Zhang, *J. Phys. Chem. C* **2011**, *115*, 21567; c) M. Sathish, T. Tomai, I. Honma, *J. Power Sources* **2012**, *217*, 85; d) T. Yoon, J. Kim, J. Kim, J. Lee, *Energies* **2013**, *6*, 4830; e) S. S. Chen, X. Qin, *NANO* **2015**, *10*, 1550081.
[9] a) D. Ma, S. Yuan, Z. Cao, *Chin. Sci. Bull.* **2014**, *59*, 6; b) C. J. Fu, G. G. Zhao, H. J. Zhang, S. Li, *Int. J. Electrochem. Sci.,* **2014**, *9*, 46; c) Y. Wang, L. Zhang, Y. Wu, Y. Zhong, Y. Hu, X. W. Lou, *Chem. Commun.* **2015**, *51*, 6921; d) X. X. Li, S. S. Zheng, L. Jin, Y. Li, P. B. Geng, H. G. Xue, H. Pang, Q. Xu, *Adv. Energy Mater.* **2018**, *8*, 25.
[10] V. Singh, D. Joung, L. Zhai, S. Das, S. I. Khondaker, S. Seal, *Prog. Mater. Sci.* **2011**, *56*, 1178.
[11] I. T. Kim, A. Magasinski, K. Jacob, G. Yushin, R. Tannenbaum, *Carbon* **2013**, *52*, 56.
[12] S. Yang, C. Cao, G. Li, Y. Sun, P. Huang, F. Wei, W. Song, *Nano Res.* **2014**, *8*, 1339.
[13] a) J. Z. Wang, C. Zhong, D. Wexler, N. H. Idris, Z. X. Wang, L. Q. Chen, H. K. Liu, *Chemistry* **2011**, *17*, 661; b) Y. Jiang, Z. J. Jiang, M. L. Liu, in *International Symposium on Material, Energy and Environment Engineering*, Vol. (ISM3E 2015), Changsha, China **2015**; c) Z. Yang, K. Qian, J. Lv, W. Yan, J. Liu, J. Ai, Y. Zhang, T. Guo, X. Zhou, S. Xu, Z. Guo, *Sci. Rep.* **2016**, *6*, 27957.
[14] X. Zhao, X. Li, S. Zhang, J. Long, Y. Huang, R. Wang, J. Sha, *J. Mater. Chem. A* **2017**, 5, 23592.
[15] J. Jiao, W. Qiu, J. Tang, L. Chen, L. Jing, *Nano Res.* **2016**, *9*, 1256.
[16] R. Li, P. Jiang, C. Gao, F. Huang, R. Xu, X. Chen, *Energy Fuels* **2016**, *31*, 188.
[17] a) S. Lone, I. W. Cheong, *RSC Adv.* **2014**, *4*, 13322; b) D. J. Han, J. H. Jung, J. S. Choi, Y. T. Kim, T. S. Seo, *Lab Chip* **2013**, *13*, 4006.
[18] C. Y. Lee, C. L. Chang, Y. N. Wang, L. M. Fu, *Int. J. Mol. Sci.* **2011**, *12*, 3263.
[19] C. Greaves, *J. Solid State Chem.* **1983**, *49*, 325.
[20] L. M. Malard, M. A. Pimenta, G. Dresselhaus, M. S. Dresselhaus, *Phys. Rep.* **2009**, *473*, 51.
[21] D. H. Wei, J. W. Liang, Y. C. Zhu, J. J. Zhang, X. N. Li, K. L. Zhang, Z. Q. Yuan, Y. T. Qian, *Electrochim. Acta* **2013**, *114*, 779.
[22] S. L. Chou, J. Z. Wang, D. Wexler, K. Konstantinov, C. Zhong, H. K. Liu, S. X. Dou, *J. Mater. Chem.* **2010**, 20.
[23] a) P. Zeng, Y. Zhao, Y. Lin, X. Wang, J. Li, W. Wang, Z. Fang, *Nanoscale Res. Lett.* **2017**, *12*, 13; b) M. Chen, J. Liu, D. Chao, J. Wang, J. Yin, J. Lin, H. Jin Fan, Z. Xiang Shen, *Nano Energy* **2014**, *9*, 364.
[24] a) S. Chen, Y. Xin, Y. Zhou, F. Zhang, Y. Ma, H. Zhou, L. Qi, *J. Mater. Chem. A* **2015**, *3*, 13377; b) J. Zhang, Y. Sun, Y. Yao, T. Huang, A. Yu, *J. Power Sources* **2013**, *222*, 59.
[25] Y. Wang, Y. Gao, J. Shao, R. Holze, Z. Chen, Y. Yun, Q. Qu, H. Zheng, *J. Mater. Chem. A* **2018**, *6*, 3659.
[26] G. Zhou, D.-W. Wang, F. Li, L. Zhang, N. Li, Z.-S. Wu, L. Wen, G. Q. Lu, H.-M. Cheng, *Chem. Mater.* **2010**, *22*, 5306.

Manuscript received: July 31, 2018
Accepted manuscript online: September 26, 2018
Version of record online: December 13, 2018